RSC Advances

RSC Advances

www.rsc.org/advances

ROYAL SOCIETY OF CHEMISTRY

www.rsc.org/advances

Journal Name

COMMUNICATION

Straightforward phase-transfer route to colloidal iron oxide nanoparticles for protein immobilization

V. Vilas-Boas,[a] N. Guldris,[b] E. Carbó-Argibay,[b] D. G. Stroppa,[b] M. F. Cerqueira,[c] B. Espiña,[b] J. Rivas,[d] C. Rodríguez-Abreu[b] and Yu. V. Kolen'ko*[b]

We report for the first time the effective transfer of hydrophobic oleate-capped iron oxide nanoparticles to aqueous phase upon treatment with base bath cleaning solution. We discuss the mechanism of the phase transfer, which involves the elimination of organic capping agent followed by ionic stabilization of the nanoparticles due to negatively charged Fe–O⁻ surface species. The resultant superparamagnetic aqueous nanocolloid shows excellent protein immobilization capability.

Iron oxide nanoparticles (NPs) are an important class of nanomaterials with useful magnetic properties, such as high Curie temperature, high saturation magnetization, and many practical biomedical applications. For example, magnetite, Fe_3O_4, and maghemite, γ-Fe_2O_3, NPs are used in cancer therapy via magnetic hyperthermia,[1] drug and gene delivery,[2, 3] magnetic separation and diagnostics,[4, 5] magnetic particle imaging,[6] as well as classical and multimodal magnetic resonance imaging.[7, 8] From the perspective of biomedical applications, iron oxide is preferred in the form of colloidally stable aqueous dispersions of monodisperse NPs exhibiting high crystallinity and high saturation magnetization. Control over particle size and shape can be achieved by colloidal synthesis methods such as thermal decomposition[9, 10] or hydrothermal/solvothermal routes[11, 12] that typically employ readily available oleate (OL) ligand as capping agent. Hence, various iron oxide NPs with tunable size and morphology have been successfully prepared. However, the drawback of the aforementioned colloidal syntheses is that the resultant NPs are hydrophobic and can be well dispersed only in apolar organic solvents. Obviously, such NPs are not suitable for biomedical application, and proper phase transfer into aqueous medium is required to render them water-dispersible.

A variety of phase-transfer protocols have been developed, which work based on electrostatic, steric or electrosteric repulsions.[13] One strategy consists of ligand exchange, where the hydrophobic surface ligand, typically oleate, is substituted by amphiphilic polymers,[14] surfactants,[15] silica shell,[16] or silane molecules.[17] Another interesting approach is coating hydrophobic NPs by amphiphilic polymers[18, 19] or bilayer shells,[20] thus rendering them dispersible in aqueous phase.

For instance, poly(ethylene glycol) (PEG) coated NPs are colloidally very stable in aqueous medium against pH and ionic strength changes, while heating of the dispersion results in NP aggregation as a consequence of low solubility of PEG in water at elevated temperatures.[21, 22] NPs transferred into water by using poly(acrylic acid) polymer or tetramethylammonium hydroxide surfactant are charged, which makes them very stable against heating but quite sensitive to ionic strength and pH of the medium. Additionally, polymers, silanes, and surfactants used for phase transfer are expensive and sometimes toxic. Hence, exploring and developing novel, simple and low cost route to transfer hydrophobic magnetic iron oxide NPs from apolar organic solvent to aqueous medium is certainly required.

Our efforts in phase transfer of monodisperse hydrophobic iron oxide NPs have been directed toward eliminating all organic capping ligands from the surface of the NPs. Specifically, we considered the possibility that elimination of organic capping ligands may be conveniently achieved through treatment of hydrophobic nanocolloids by a base bath cleaning solution, which is an inherent part of any chemical laboratory. We envisioned that, in this way, water-dispersible iron oxide NPs should be formed as a result of ionic stabilization.[23] This straightforward route offers one principle advantage over a traditional polymer and surfactant routes, namely, it produces a nanocolloid free of organic coating, and thus results in a greater content of magnetic material in the final product. To understand the changes that the nanoparticles undergo during base-bath-assisted phase transfer, we investigated the structure and magnetic properties of the resultant water-

a. UCIBIO-REQUIMTE, Laboratory of Toxicology, Biological Sciences Department, Faculty of Pharmacy, University of Porto, 4050–313 Porto, Portugal.
b. International Iberian Nanotechnology Laboratory, 4715–330 Braga, Portugal. E-mail: yury.kolenko@inl.int
c. Center of Physics, University of Minho, Braga 4710–057, Portugal.
d. Department of Applied Physics, University of Santiago de Compostela, Santiago de Compostela 15782, Spain.

dispersible nanocolloids, which we detail in this communication.
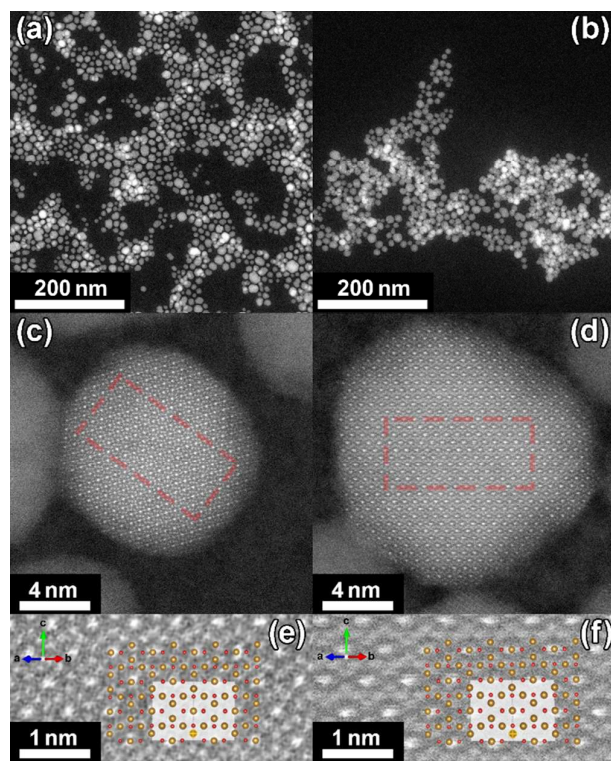
Fig. 1. Comparison of low-magnification, [110] high- and atomic-resolution HAADF-STEM images together with the corresponding structural models (Fe atoms = yellow, O atoms = red) for **OL-HT** (a, c, e) and **OL-HT-BB** (b, d, f) nanocolloids. The indicated square areas in (c) and (d) are shown enlarged in (e) and (f), respectively.

OL-capped magnetite nanocolloid (entry **OL-HT**, Fig. S1a, ESI†) was synthesized by hydrothermal method reported elsewhere.[24] As shown in Fig. 1a, the as-prepared nanocolloid consists of highly crystalline NPs with an average particle diameter of 10.5 ± 5.2 nm with a 95.45% confidence level, i.e. 2σ. Treating this hydrophobic nanocolloid with KOH base bath cleaning solution for 24 h at room temperature followed by separation by centrifugation and purification by ethanol provides a brown aqueous nanocolloid (entry **OL-HT-BB**, Fig. S1b, ESI†) in nearly 70% isolated yield. High-angle annular dark-field scanning transmission electron microscopy (HAADF-STEM) images show that this phase-transfer product consists of many highly crystalline NPs similar to those in the initial **OL-HT** nanocolloid (Fig. 1b). Additionally, no dramatic changes in particle size or shape are observed with an average particle diameter of **OL-HT-BB** estimated to be 11.1 ± 5.2 nm. Notably, the NPs are not well separated spatially from each other as in the case of **OL-HT** NPs, which is most likely due to their aggregation during the drying of aqueous NP dispersion on the carbon-coated TEM grid.

To test whether the atomic structure of the NPs is affected during phase transfer, we carried out a morphology characterization using atomic resolution STEM. Figs. 1b and 1c show a comparison between the HAADF-STEM images of the NPs before and after phase transfer. These data confirm that the atomic structures of the initial and the resultant NPs are comparable. The NPs have cubic inverse-spinel structure type, space group Fd-$3m$ (Figs. 1e and 1f). Notably, we cannot conclusively distinguish between Fe_3O_4 and γ-Fe_2O_3 iron oxide phases using our atomic resolution TEM data, or even with electron energy loss spectroscopy (EELS) studies.[25] Specifically, EELS spectra from both **OL-HT** and **OL-HT-BB** NPs are extremely similar and the changes in Fe L_3/L_2 ratio and in O proportion are not significant (Fig. S2, ESI†). Therefore, we conclude that Fe_3O_4 and γ-Fe_2O_3 are indistinguishable by the used techniques. This is most likely due to the isostructural nature of these two compounds having similar cubic unit cell parameters (a = 8.396 Å for Fe_3O_4 and a = 8.352 Å for γ-Fe_2O_3), forming Fe_3O_4–γ-Fe_2O_3 solid solutions.[24]

Next, we investigated the influence of the developed phase-transfer route on the structural properties of the resultant iron oxide NPs. Powder X-ray diffraction (XRD) confirmed that both **OL-HT** and **OL-HT-BB** samples have cubic inverse-spinel structure (Fig. S3, ESI†). No remarkable changes are observed after phase transfer. Notably, we were not able to conclusively distinguish between Fe_3O_4 and γ-Fe_2O_3 using XRD, which is consistent with the aforementioned electron microscopy study. γ-Fe_2O_3 and Fe_3O_4 have very similar crystal structures, and the small size of the NPs results in very broad XRD peaks, rendering phase-composition studies difficult. In contrast to XRD, Raman scattering can unambiguously detect the different iron oxide phases, because different polymorphs show distinct Raman-active phonon modes.[26] The main difference between the Raman spectra of Fe_3O_4 and γ-Fe_2O_3 stems from the different position of the most intense A_{1g} phonon modes.[24] We compared the ratio ($R = I$(666 cm^{-1})/I(715 cm^{-1})) of the intensity of the A_{1g} mode of Fe_3O_4 to the intensity of the A_{1g} mode of γ-Fe_2O_3. For **OL-HT** NPs, R is 1.5, indicating the coexistence of both phases, with Fe_3O_4 as the abundant one (Fig. S4a, ESI†). This is in good agreement with our previous studies, wherein we determined that the structure of hydrothermally-synthesized **OL-HT** NPs is best understood as a Fe_3O_4–γ-Fe_2O_3 solid solution.[19] In contrast to **OL-HT**, **OL-HT-BB** has a lower R value of 0.93 (Fig. S4b, ESI†). These data suggest that base-bath-assisted phase transfer leads to the slight oxidation of the initial Fe_3O_4–γ-Fe_2O_3 solid solution NPs to one with large maghemite composition. We speculate that this oxidation within 24 h of the treatment is driven by oxygen from air. It seems clear that the removal of the protective OL capping ligands from the NPs results in direct exposure of their surfaces to the oxidative base-bath conditions.

We employed vibrating sample magnetometry (VSM) at room temperature to investigate the magnetic field dependence of magnetization [$M(H)$] for the iron oxide NPs. The $M(H)$ data in Fig. 2 show that both nanocolloids exhibit superparamagnetic behaviour without any signature of coercivity, as manifested by the lack of hysteresis loops. The saturation magnetization (M_s) of **OL-HT-BB** is 72.7 emu/g, which is just slightly lower than that of the initial **OL-HT** (73.8 emu/g). These large M_s values stem from the high crystallinity

RSC Advances

COMMUNICATION

and increased particle size.[19, 24] The small decrease in M_s after phase transfer correlates well with the observed oxidation of Fe_3O_4–γ-Fe_2O_3 **OL-HT** into largely γ-Fe_2O_3 **OL-HT-BB**, since bulk γ-Fe_2O_3 (80 emu/g) exhibits lower M_s than bulk Fe_3O_4 (92 emu/g).[27] Nevertheless, the M_s of hydrophilic **OL-HT-BB** obtained by our newly developed phase-transfer route is superior to that of other Fe_3O_4 or Fe_2O_3 NPs synthesized by the majority of methods,[28, 29] and the superparamagnetic state does not change with the phase transfer.
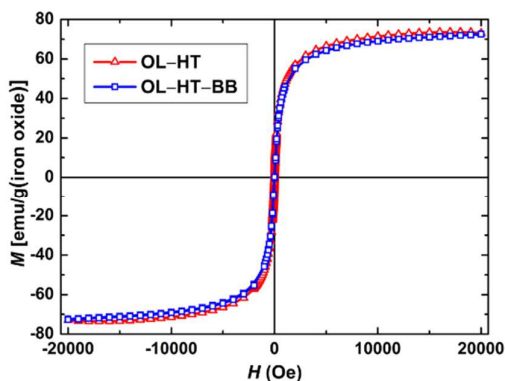

Fig. 2. Room-temperature $M(H)$ dependence data for **OL-HT** and **OL-HT-BB** nanocolloids.

Having investigated structural, microstructural, and magnetic properties before and after phase transfer, we further probed NP capping with the aim of elucidating mechanistic details of our phase-transfer protocol. Thermogravimetric and differential scanning calorimetry analysis (TGA-DSC) of the powdered **OL-HT-BB** demonstrates that the sample contains only a small amount of organic phase, as shown by ca. 2% weight loss between 300 and 750 °C (Fig. S5, ESI†), the temperature range of OL decomposition.[19] Notably, this value is significantly lower compared to the theoretically calculated ones of 9.6% and 18.3% assuming full OL coverage of 11.1-nm iron oxide NPs (Fig. S6, ESI†), evidencing the loss of organic phase. Significant elimination of OL capping after base-bath treatment is also confirmed by Fourier transform infrared spectroscopy (FTIR, Fig. S7, Table S1, ESI†). We presume that the colloidal stability of **OL-HT-BB** results from the effective cleavage of the OL ligands by KOH from the NP surface in the base bath followed by the formation of ionically-stabilized NPs with negatively charged Fe–O⁻ surface species.[23]

We tested our hypothesis of the ionic stabilization by conducting Zeta potential measurements at different pH values. **OL-HT-BB** displays negative Zeta potential of –89 mV at pH 9, –10 mV in phosphate buffer pH 7.4, and +13 mV in MES [(2-(N-morpholino)ethanesulfonic acid)] buffer pH 5.1. These results corroborate that the mechanism of our convenient base-bath-assisted phase transfer proceeds through the elimination of the surface capping ligands followed by subsequent formation of negative-charge-surrounded iron oxide NPs.[30] In water at basic pH, the NPs exhibit electrostatic

repulsions that render them colloidally stable (Fig. S1b, ESI†). Hence, as-prepared aqueous nanocolloid is pH sensitive and has to be stored at pH ≥ 8.

Aiming at employing magnetic **OL-HT-BB** for biomedical applications, we examined the potential of our aqueous nanocolloids for proteomic analysis.[31] As a proof-of-concept, we chose to study the immobilization of bovine serum albumin (BSA) protein onto the magnetic NPs. For example, crosslinked BSA-coated iron oxide contrast agents for MRI visualization of intracranial glioma was realized with this reasonably cheap and available protein.[32] In addition, the stability and biocompatibility of the NPs typically improve when loaded with BSA.[33]
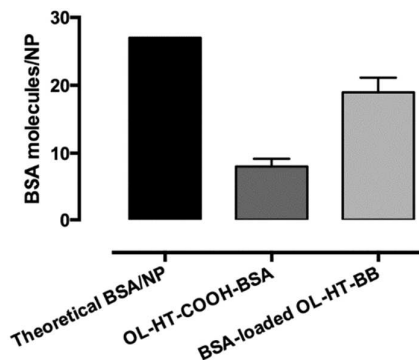

Fig. 3. Comparison of BSA loading through physical adsorption on **OL-HT-BB** NPs with a covalently bonded control **OL-HT-COOH** NPs as reference, which indicates significantly higher BSA immobilization in the case of **OL-HT-BB** NPs ($P < 0.05$).
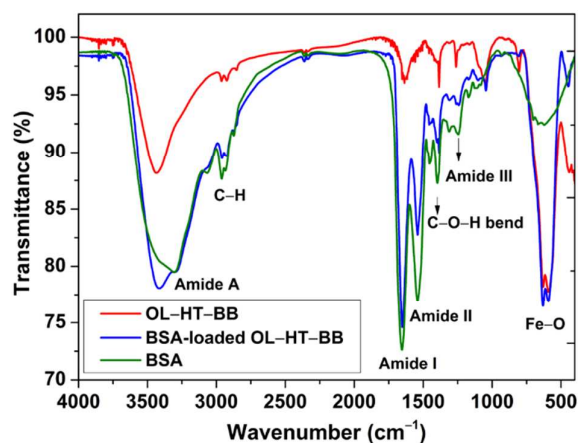

Fig. 4. Comparison of the FTIR spectra of lyophilized **OL-HT-BB**, BSA-loaded **OL-HT-BB** and BSA (Table S1, ESI†).

We expected our non-coated, charged **OL-HT-BB** NPs to be suitable for efficient anchoring of protein molecules, and therefore, carried out BSA immobilization experiments. We found that incubation of **OL-HT-BB** NPs in BSA solution for 3 h at 4 °C (ESI†) led to protein loading of an average of 19 BSA molecules per NP (Fig. 3). This value turned out to be slightly lower than the theoretically estimated 27 BSA/NP assuming monolayer coverage. To elucidate the efficiency of our loading procedure, we also prepared BSA-bearing **OL-HT** NPs using the

known carbodiimide/*N*-hydroxysulfosuccinimide (EDC/sulfo-NHS) method, where BSA is covalently bonded to the NP surface (ESI†). We found that BSA loading using EDC/sulfo-NHS method provides an average 8 BSA/NP (ESI†), which is significantly lower than in the case of **OL-HT-BB** (Fig. 3).

To characterize BSA binding, we performed an FTIR study of BSA, **OL-HT-BB**, and BSA-loaded **OL-HT-BB** samples lyophilized from the respective aqueous dispersions (Fig. 4). The spectrum of BSA-loaded **OL-HT-BB** features the characteristic amide I, II, and III bands of BSA, as well as the Fe−O band for iron oxide NPs, clearly confirming the presence of the protein on the NP surface. We presume that BSA is physisorbed on the **OL-HT-BB** NPs, most likely via Coulomb forces.[34] Specifically, incubation of **OL-HT-BB** NPs in BSA solution is carried out in Millipore water at pH 5.3 (ESI†). It is known that the isoelectric point of BSA is at pH = 4.7,[35, 36] therefore at this slightly acidic pH of 5.3 the BSA molecules are negatively charged. In contrast, as shown by the aforementioned Zeta potential measurements, the **OL-HT-BB** NPs at pH 5.3 are positively charged. Consequently, we propose that BSA-loaded iron oxide NPs are formed as a result of electrostatic interactions.
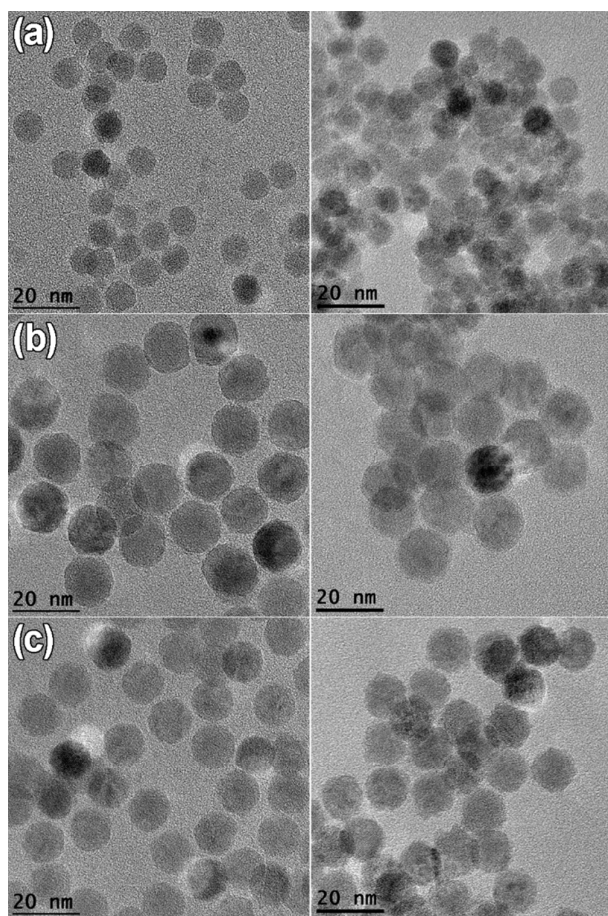
Fig. 5. TEM images showing a series of control phase-transfer experiments for monodisperse iron oxide NPs with sizes of 9.3 ± 1.2 nm (a), 8.7 ± 1.2 nm (b), 13.2 ± 1.1 nm (c), 13.2 ± 1.4 nm (d), 15.8 ± 1.7 nm (e), and 14.8 ± 1.7 nm (f) prepared by thermal decomposition of Fe(OL)$_3$. Left panels (a, c, e) demonstrate the initial hydrophobic NPs, whereas right panels (b, d, f) show the respective NPs after phase transfer to aqueous media using base-bath treatment. The confidence levels are 95.45%, i.e. 2σ.

Finally, to extend the use of our convenient phase-transfer route to monodisperse magnetic NPs, we prepared a series of iron oxide NPs using thermal decomposition of Fe(OL)$_3$ complex (ESI†).[9] Monodisperse hydrophobic NPs with average diameters of 9.3 ± 1.2 nm, 13.2 ± 1.1 nm, and 15.8 ± 1.7 nm were synthesized and successfully transferred to aqueous medium without apparent morphological or structural changes (Figs. 5 and S8 (ESI†)). Obviously, our novel phase transfer can be successfully employed to obtain aqueous monodisperse magnetic nanocolloids. Hence, we expect this efficient protocol to find broad application in phase transfer chemistry in the field of nanomedicine.

Conclusions

In summary, we have developed a novel convenient protocol to transfer hydrophobic oleate-capped iron oxide NPs from organic to aqueous phase. Our characterization data provide general evidence of the effective oleate-ligand removal under base-bath conditions followed by formation of ionically-stabilized NPs, rendering them dispersible in aqueous medium. The outstanding physical adsorption of protein by these hydrophilic NPs without the need for functionalization highlights the potential of the system in sample preparation for proteomics. This novel phase-transfer route can be extended to obtain monodisperse aqueous nanocolloids of various materials for further use in biomedical applications.

Acknowledgements

Notes and references

1. M. Johannsen, U. Gneveckow, L. Eckelt, A. Feussner, N. Waldofner, R. Scholz, S. Deger, P. Wust, S. A. Loening and A. Jordan, *Int. J. Hyperthermia*, 2005, 21, 637-647.
2. S. C. McBain, H. H. P. Yiu and J. Dobson, *Int. J. Nanomed.*, 2008, 3, 169-180.
3. J. R. Ohlfest, A. B. Freese and D. A. Largaespada, *Curr. Gene Ther.*, 2005, 5, 629-641.
4. I. Safarik and M. Safarikova, *J. Chromatogr. B*, 1999, 722, 33-53.
5. M. E. Davis, Z. Chen and D. M. Shin, *Nat. Rev. Drug Discov.*, 2008, 7, 771-782.
6. B. Gleich and R. Weizenecker, *Nature*, 2005, 435, 1214-1217.

RSC Advances Accepted Manuscript

7. J. S. Choi, J. H. Lee, T. H. Shin, H. T. Song, E. Y. Kim and J. Cheon, *J. Am. Chem. Soc.*, 2010, 132, 11015-11017.
8. Y.-X. J. Wang, *Quant. Imaging Med. Surg.*, 2011, 1, 35-40.
9. J. Park, K. J. An, Y. S. Hwang, J. G. Park, H. J. Noh, J. Y. Kim, J. H. Park, N. M. Hwang and T. Hyeon, *Nat. Mater.*, 2004, 3, 891-895.
10. S. H. Sun, H. Zeng, D. B. Robinson, S. Raoux, P. M. Rice, S. X. Wang and G. X. Li, *J. Am. Chem. Soc.*, 2004, 126, 273-279.
11. T. Taniguchi, K. Nakagawa, T. Watanabe, N. Matsushita and M. Yoshimura, *J. Phys. Chem. C*, 2009, 113, 839-843.
12. X. Wang, J. Zhuang, Q. Peng and Y. D. Li, *Nature*, 2005, 437, 121-124.
13. J. Yang, J. Y. Lee and J. Y. Ying, *Chem. Soc. Rev.*, 2011, 40, 1672-1696.
14. Y. L. Xu, Y. Qin, S. Palchoudhury and Y. P. Bao, *Langmuir*, 2011, 27, 8990-8997.
15. V. Salgueirino-Maceira, M. A. Correa-Duarte and M. Farle, *Small*, 2005, 1, 1073-1076.
16. M. Zhang, B. L. Cushing and C. J. O'Connor, *Nanotechnology*, 2008, 19.
17. M. Bloemen, W. Brullot, T. T. Luong, N. Geukens, A. Gils and T. Verbiest, *J. Nanopart. Res.*, 2012, 14.
18. G. Palui, F. Aldeek, W. T. Wang and H. Mattoussi, *Chem. Soc. Rev.*, 2015, 44, 193-227.
19. Y. V. Kolen'ko, M. Bañobre-López, C. Rodríguez-Abreu, E. Carbó-Argibay, A. Sailsman, Y. Piñeiro-Redondo, M. F. Cerqueira, D. Y. Petrovykh, K. Kovnir, O. I. Lebedev and J. Rivas, *J. Phys. Chem. C*, 2014, 118, 8691-8701.
20. A. Prakash, H. G. Zhu, C. J. Jones, D. N. Benoit, A. Z. Ellsworth, E. L. Bryant and V. L. Colvin, *ACS Nano*, 2009, 3, 2139-2146.
21. A. S. Karakoti, S. Das, S. Thevuthasan and S. Seal, *Angew. Chem. Int. Ed.*, 2011, 50, 1980-1994.
22. F. Zhang, E. Lees, F. Amin, P. R. Gil, F. Yang, P. Mulvaney and W. J. Parak, *Small*, 2011, 7, 3113-3127.
23. R. Massart, *IEEE Trans. Magn.*, 1981, 17, 1247-1248.
24. Y. V. Kolen'ko, M. Banobre-Lopez, C. Rodriguez-Abreu, E. Carbo-Argibay, F. L. Deepak, D. Y. Petrovykh, M. F. Cerqueira, S. Kamali, K. Kovnir, D. V. Shtansky, O. I. Lebedev and J. Rivas, *J. Phys. Chem. C*, 2014, 118, 28322-28329.
25. C. Colliex, T. Manoubi and C. Ortiz, *Phys. Rev. B*, 1991, 44, 11402-11411.
26. A. M. Jubb and H. C. Allen, *ACS Appl. Mater. Interfaces*, 2010, 2, 2804-2812.
27. R. M. Cornell and U. Schwertmann, *The Iron Oxides: Structure, Properties, Reactions, Occurences and Uses*, Wiley-VCH, Weinheim, Germany, 2 edn., 2003.
28. S. Laurent, D. Forge, M. Port, A. Roch, C. Robic, L. V. Elst and R. N. Muller, *Chem. Rev.*, 2008, 108, 2064-2110.
29. A. H. Lu, E. L. Salabas and F. Schuth, *Angew. Chem. Int. Ed.*, 2007, 46, 1222-1244.
30. R. Costo, V. Bello, C. Robic, M. Port, J. F. Marco, M. P. Morales and S. Veintemillas-Verdaguer, *Langmuir*, 2012, 28, 178-185.
31. Y. Li, X. M. Zhang and C. H. Deng, *Chem. Soc. Rev.*, 2013, 42, 8517-8539.
32. M. A. Abakumov, N. V. Nukolova, M. Sokolsky-Papkov, S. A. Shein, T. O. Sandalova, H. M. Vishwasrao, N. F. Grinenko, I. L. Gubsky, A. M. Abakumov, A. V. Kabanov

and V. P. Chekhonin, *Nanomed. Nanotechnol. Biol. Med.*, 2015, 11, 825-833.
33. J. Jenita, V. Chocalingam and B. Wilson, *Int. J. Pharma. Investig.*, 2014, 4, 142-148.
34. R. V. Mehta, R. V. Upadhyay, S. W. Charles and C. N. Ramchand, *Biotechnol. Tech.*, 1997, 11, 493-496.
35. S. R. Ge, S. Kojio, A. Takahara and T. Kajiyama, *J. Biomat. Sci. Polym. Ed.*, 1998, 9, 131-150.
36. S. Salgin, U. Salgin and S. Bahadir, *Int. J. Electrochem. Sci.*, 2012, 7, 12404-12414.

A table of contents entry
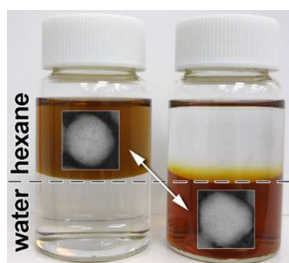
Removal of hydrophobic ligand enables a convenient phase-transfer route to aqueous magnetic nanocolloid that shows excellent protein immobilization capability.